Periodica Polytechnica
Mechanical Engineering

61(3), pp. 247-254, 2017
https://doi.org/10.3311/PPme.10816

RESEARCH ARTICLE

Investigation on the Nonconstant Behavior of a Vortex Flow Meter with Narrow Gauge Pipe via Conducting Measurements and Numerical Simulations

Bence Fenyvesi[1*], Csaba Horváth[1]

Received 30 March 2017; accepted after revision 31 May 2017

Abstract

Vortex shedding flowmeters can be used for a wide range of flow measurement applications with various kinds of fluids. The critical point in applying this method comes from the assumption that the Strouhal number is constant for the given Reynolds number range. In some cases – typically regarding flowmeters with narrow gauge pipes –, this assumption is only partially met, thus limiting the widespread use of these instruments in certain industrial appliances. The paper presents a diagnostic investigation on the effects of this nonconstant behavior. The method elaborated in this report can be applied to vortex flowmeters with narrow gauge pipes. In these instruments – usually due to the narrow cross-sections of the gauge pipe – measurement possibilities are limited, thus it is not possible for the user to determine the effects of the nonconstant behavior. To conduct these investigations, a calibration rig was designed and assembled. The presented diagnostic method combines measurements and numerical simulations. The results of the investigations can be used in the data processing phase, in order to reduce the uncertainty of the volume flow rate measured by vortex flowmeters.

Keywords

vortex-shedding, flow meter, narrow gauge pipe, nonconstant effect

[1] Department of Fluid Mechanics,
Faculty of Mechanical Engineering,
Budapest University of Technology and Economics
Bertalan Lajos u. 4-6. H-1111 Budapest, Hungary

[*] Corresponding author, e-mail: fenyvesi@ara.bme.hu

1 Introduction

Uncertainty is one of the most important criteria in flow measurement. In 2007, vortex flowmeters received the approval of the American Petroleum Institute (API) for use in custody-transfer applications [1]. Though this concerns specifically liquid, steam and gas applications, there are still remaining challenges that require further research.

The instrument's measurement principle states, that when placing a body in a flow, which can be characterized by a specific Reynolds-number (*Re*), a von Kármán vortex street will be shed from the surface of the body. Assuming that the Strouhal number (*Str*) is constant on this range, the vortex shedding frequency (*f*) is proportional to the Strouhal number, and hence to the volume flow rate of the inspected flow [2]. Under these ideal conditions, flow meters would be having completely linear characteristics, therefore the volume flow rate would be proportional to the vortex shedding frequency for the entire measurement range.

As shown in Eq. (1) and (2), apart from the kinematic viscosity (ν) and the velocity of the flow (*u*), the Reynolds and Strouhal numbers are highly dependent on the width of the bluff body's frontal surface (*d*), which is embedded in the measurement section (gauge pipe) of the flowmeter.

$$Re = \frac{u \cdot d}{\nu} \tag{1}$$

$$Str = \frac{f \cdot d}{u} \tag{2}$$

When our team calibrated vortex meters for industrial use, a trend in the deviation from the expected constant behavior was noticed while studying the calibration diagrams. Previous research has shown, that the Strouhal number is not always independent of the Reynolds number [3, 4], and being the cause of the nonconstant behavior, it can have an effect on the uncertainty of the instrument.

While many previous studies presented general investigations on this nonconstant behavior of vortex flow meters, the aim of the present study is to extend the research to instruments with narrow gauge pipes. In these devices, due to the small size of the measurement section, the vortex shedding

frequency cannot be measured directly in most cases. Since without knowing the value of this frequency, the Strouhal number cannot be obtained, the effects of the nonconstant behavior cannot be determined by simply using the data provided by the device, hence demanding a novel approach and use of alternative diagnostic methods.

In order to study the phenomenon, a calibration rig with enhanced accuracy was designed. By combining measurement data and results of various numerical simulations, a diagnostic method was developed a for calculating the vortex shedding frequency.

2 Calibration

2.1 Measurement device

The device used during the investigations is an SMC PF3W704S-F03-FT-M type vortex flowmeter [5]. As shown in Fig. 1, the cross-section of the gauge pipe is an oval (race-track) shaped one, and has a width (e) – height (h) ratio of 1.8. The body embedded in the gauge pipe is a special, "delta-shaped" element. The ratio of the width of the body's frontal surface (d) and the pipe width (blockage ratio) is 0.28.

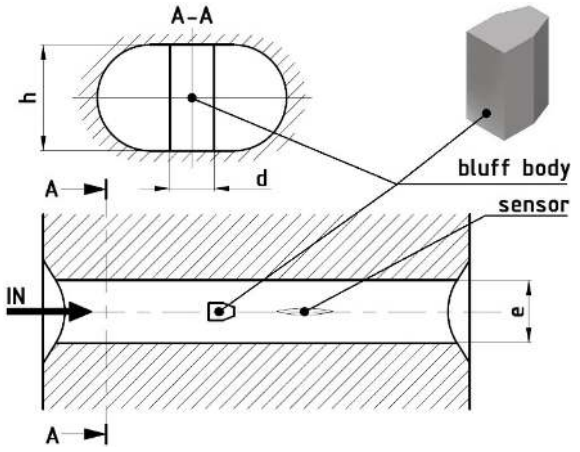

Fig. 1 Horizontal and vertical cross-sections of the flowmeter's gauge pipe

The device consists of separate blocks. After a specified length of straight piping and standard pipe thread connection, the flow enters the gauge pipe. The sensor downstream to the bluff body measures the vortex shedding frequency, and the calculated volume flow rate can be seen on a digital display, which shows the value with 0.01 liter/min accuracy. After the gauge pipe, a second sensor measures the temperature of the fluid, which can also be seen on the display. The last block of the instrument contains a globe valve for the precise adjustment of the desired flow rate.

The rated flow range of the device is 0.5 to 4 liter/min, the uncertainty of the flowmeter is ±3 % for the full scale of the measurement range. The instrument's operating pressure range is 0 to 1 MPa, the operating temperature range is 0 to 90 °C. The measurements are to be carried out using distilled water as working fluid, in order to avoid corrosion in the system.

The flow rate characteristics (pressure loss) diagram of the device, and further specifications can be found in the manufacturer's catalog [5].

2.2 Calibration set-up

Considering the described parameters and the requirements of the related standards [6], an open-loop calibration rig was designed. The schematic diagram of this calibration system is shown in Fig. 2.

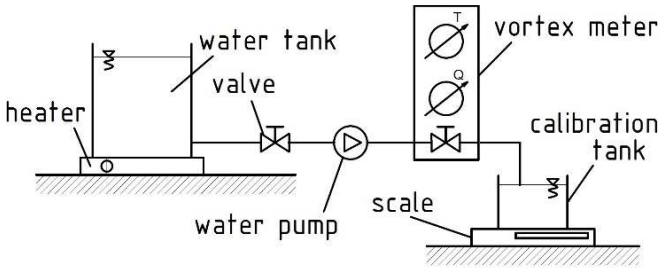

Fig. 2 The calibration rig designed for the investigation

The working fluid is contained in a tank. In order to minimize the error, caused by the decrease in pressure difference, the level of the water was kept the same, and a tank with relatively wide diameter was used. To keep the water-density (ρ) constant, the fluid-temperature was also kept constant during the measurements with a heater unit. The required flow rate for each of the 10 measurement points was set using the frequency inverter of the circulation pump the valve downstream to the tank, and the globe valve built into the vortex meter.

After leaving the instrument, the water flows into the calibration tank. Changes in the weight of this tank (Δm) are recorded by a precise scale, and the elapsed time (Δt) is also measured. The volume flow rate can be calculated using the formula shown in Eq. (3).

$$Q = \frac{\Delta m}{\Delta t \cdot \rho} \tag{3}$$

Compared to the vortex meter, which has an uncertainty of ±3 %, the required uncertainty of the calibration rig is ±1% or below [6]. Since it is important to know the expected accuracy before assembling the calibration rig, estimated test values were used during the design process to predict the uncertainty of the set-up. The values and the uncertainties pertaining to these quantities can be found in Table 1.

Table 1 Test values and uncertainties of measured and derived quantities

Name	Test value	Value of uncertainty	Unit
Δm	3500	± 2.5	[g]
Δt	250	± 0.1	[s]
ρ	995.18	± 0.5	[kg/m^3]

The uncertainties regarding the measurements of Δm and Δt were determined according to the accuracies of their measurement devices. The value of the density of the working fluid was obtained according to the properties of water at 30 °C [7]. During the determination of its uncertainty, the effect of the uncertainty of the temperature [7] was also taken into account, and the final value was obtained via conservative estimation.
In this article, uncertainties of calculated values are determined using the formula shown in Eq. (4) [8],

$$\delta R = \sqrt{\left(\frac{\partial R}{\partial x_1}\cdot \delta x_1\right)^2 + \left(\frac{\partial R}{\partial x_2}\cdot \delta x_2\right)^2 + \ldots,} \tag{4}$$

where R is the final value of the given calculation, and x_i are the variables present in the formula.

Based on the test values listed in Table 1, the estimated relative uncertainty of the set-up is 0.192 %. As the test flow rate is close to the minimum of the measurement range (0.84 liter/min), the results, regarding the accuracy can be considered satisfactory. The calibration rig has been built according to plan.

2.3 Calibration diagram

After assembling the equipment, multiple measurement cycles were performed at various fluid temperatures, in order to minimize the effect of non-foreseeable or random occurrences in the behavior of the vortex meter. Each measurement was performed sequentially, in one cycle, 10 different volume flow rate values were set along the measurement range of the instrument. The temperature of the working fluid was kept constant during a measurement cycle.

As there was no change in the behavior of the device for the various calibration settings, results will be presented using the data acquired at a water temperature of 30 °C. The calculation of the volume flow rate measured by the calibration rig was determined using the formula presented in Eq. (3).

The calibration diagram together with the error bars of the calibration points is shown in Fig. 3. The measurement points have a close fit to the trendline, however, a diversion from the line can also be noticed. This nonconstant behavior will be investigated hereafter.

The relative difference (ε) between the volume flow rate, measured by the vortex meter (Q_{vortex}), and the values determined using the calibration rig is calculated according to the formula in Eq. (5).

$$\varepsilon = \frac{Q - Q_{vortex}}{Q} \tag{5}$$

The diagram of relative difference is shown in Fig. 4. The accuracy of the vortex meter varies along the measurement range. The nonconstant trend shown in the calibration diagram can also be noticed here.

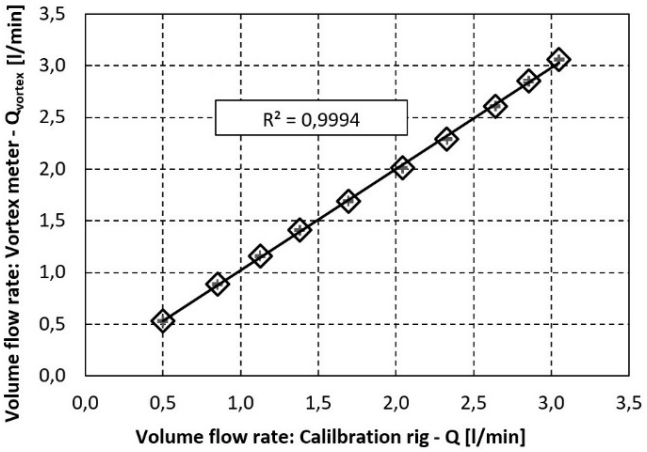

Fig. 3 The calibration diagram on 30°C temperature

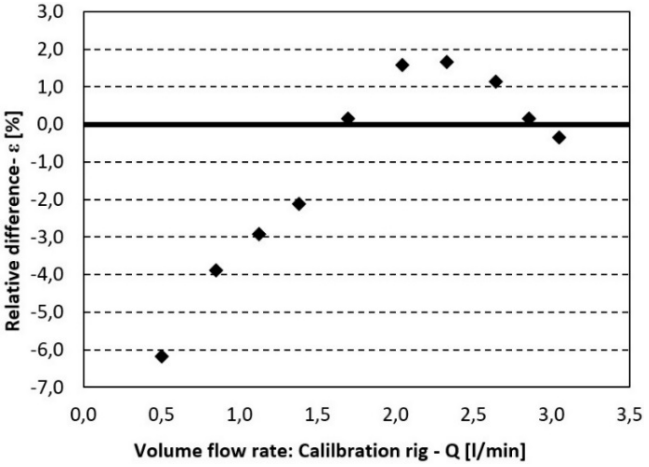

Fig. 4 Relative difference between the vortex meter and the calibration rig

3 Reynolds – Strouhal diagram

3.1 Reynolds number

Using geometric properties and volume flow rate data from the calibration process, the Reynolds number can be determined. According to Eq. (6), the area of the cross section of the gauge pipe at the bluff body (A) is 8.39 mm^2.

$$A = \frac{h^2\cdot\pi}{4} + h\cdot(e - h - d) \tag{6}$$

Velocities (u) in the cross section were calculated using the formula shown in Eq. (7).

$$u = \frac{Q}{A} \tag{7}$$

Kinematic viscosity of the fluid was determined according to the properties of water at 30 °C [9]. Uncertainty of geometric quantities and the kinematic viscosity are presented in Table 2.

Table 2 Defined and calculated uncertainties of values

Name	Value of uncertainty	Unit
d, h, e	1	[mm]
A	0.0462	[mm^2]
v	$1 \cdot 10^{-9}$	[m^2/s]

The Reynolds number for each velocity was calculated according to Eq. (1). The values and uncertainties of this calculation are presented in Fig. 12, and Table 4.

3.2 Vortex shedding frequency

In order to calculate the Strouhal number, the vortex shedding frequency is needed. As it cannot be determined using the outputs of the vortex meter, application of an alternative method is necessary.

The method presented herein assumes, that if the value of the Strouhal and Reynolds numbers would be known in one measurement point, their values for the remaining measurement points could be determined by proportional calculations. The method is presented in detail in Section 3.6. To obtain the vortex shedding frequency, numerical simulations were conducted.

Since the gauge pipe of the flowmeter is relatively narrow, it's dimensions are comparable to the thickness of the boundary layer at the pipe-wall and the size of the vortices shed from the surface of the bluff body. Furthermore, based on the literature [10, 11], it can be expected, that due to its blockage ratio of 0.28, the flow conditions and the vortex shedding properties in the gauge pipe will be different from the flow conditions around a body placed in a broad (quasi-infinite) flow field. To determine this difference for the current bluff body, two numerical models were created, one with a broad flow-field, and one identical to the gauge pipe of the flowmeter. Henceforward the broad flow-field model is referred as the "infinite", and to the model of the gauge pipe as the "gauge pipe" case.

Preliminary investigations were conducted in order to determine the nature of the difference between the two cases (see section 3.4.), and to provide data for validation of the numerical method used during the simulations. Since measurement results are solely available for the infinite model, conducted with a bluff body similar to the one embedded in the flowmeter [2], the broad flow-field simulation results will be used for validation of the numerical method.

3.3 Numerical models

The two-dimensional numerical models created to investigate the flow conditions of the infinite and the gauge pipe cases can be seen in Fig. 5.

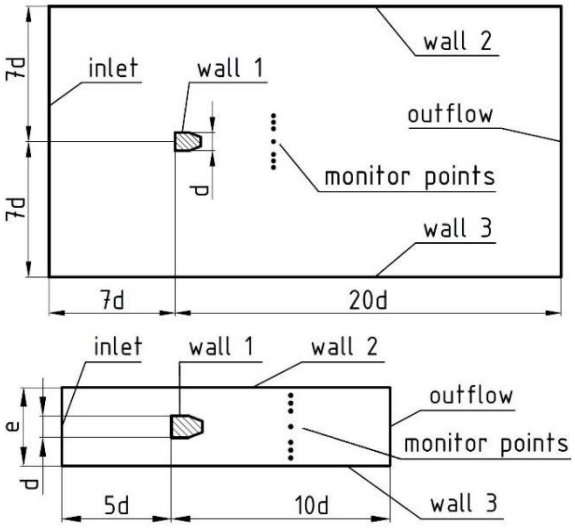

Fig. 5 Numerical models of the flow-fields

For the infinite model, the side-walls of the computational domain (*wall 2, wall3*) have no shear constants (frictionless), while the shear constant on the surface of the bluff body (*wall1*) is 0.1, In the model of the gauge pipe, all three walls have *No Slip Wall* boundary conditions with 0.1 shear constants. The velocity profile at the *Velocity Inlet* is a uniform one. Velocity magnitudes and Reynolds numbers are set to match the values corresponding to the volume flow rates of the measurement points recorded during the calibration (see Table 4).

The dimensions of the flow-fields are multiples of the width of the body's frontal surface. Seven monitor points represent the sensor downstream the bluff body.

The numerical grids are shown in Fig. 6 and Fig. 7. Both grids were created using ANSYS ICEM package.

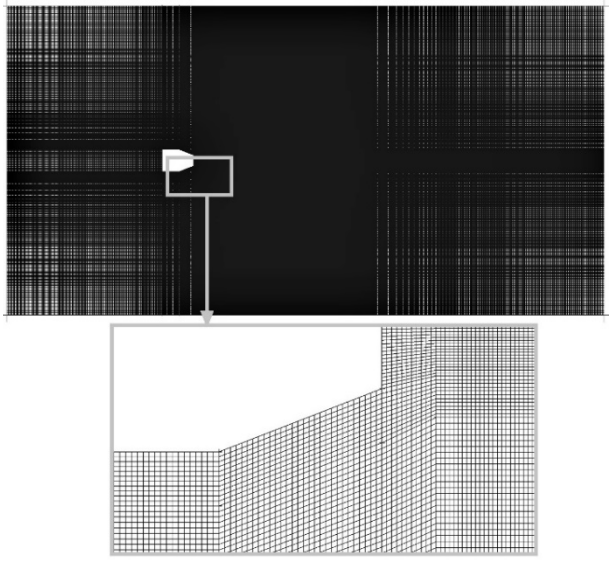

Fig. 6 Numerical grid of the infinite flow-field

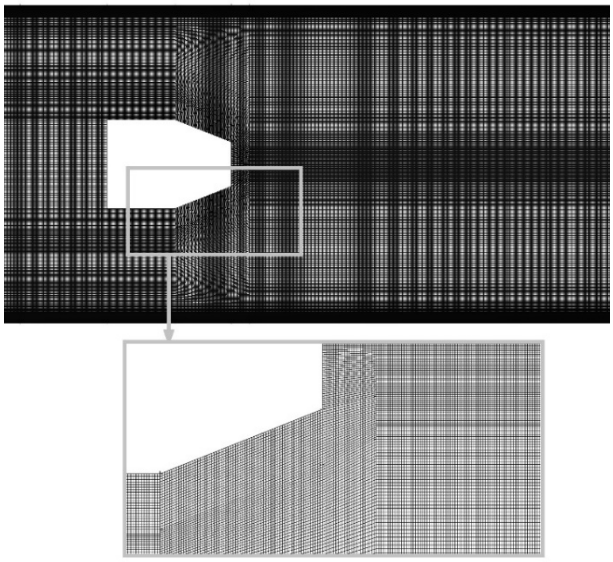

Fig. 7 Part of the numerical grid of the gauge pipe flow-field

The computational domains have 12 sub-blocks, the grids are finer in the surroundings of the bluff body, and are linearly coarsened towards the boundaries of the domain. For the gauge pipe model, the mesh is also fine near the side walls of the domain (*wall 2, wall 3*), to capture the effects of wall-friction. For the infinite case, there is no wall-friction, thus there is no finer mesh along the side wall. The mesh size is 450 000 cells for both cases.

For the maximum desired Reynolds number (10 000), y+ values in the whole flow-field would be below 1, hence both meshes can be used for further simulations and calculations.

3.4 Preliminary investigation

To determine the difference between the presented cases, preliminary simulations are needed. Transient numerical simulations were accomplished for both cases, using the finite volume based commercial CFD software, ANSYS Fluent. According to the recommendations of the related literature [12], the *k-ω SST* turbulence model was used. Material properties were set in accordance with properties of distilled water at a temperature of 30 °C. Velocity magnitude was set to 2.74 m/s, resulting in a Reynolds number of 4910.

Time step for the infinite test case was set to 10^{-5} s, and $6 \cdot 10^{-6}$ for the model of the gauge pipe, with 20 iteration cycles in every time step. Using these time steps, the value of the Courant number could be kept under 1 for the whole computational domain. The simulations were carried out with the application of double precision solving methods after standard initialization.

Values of static pressure and velocity magnitude were registered in an output file in the seven monitor points for every time step. A monitor point – through which the centers of the vortices moved – was chosen for further evaluation. Fig. 8 shows the change in velocity magnitude in this point for both cases.

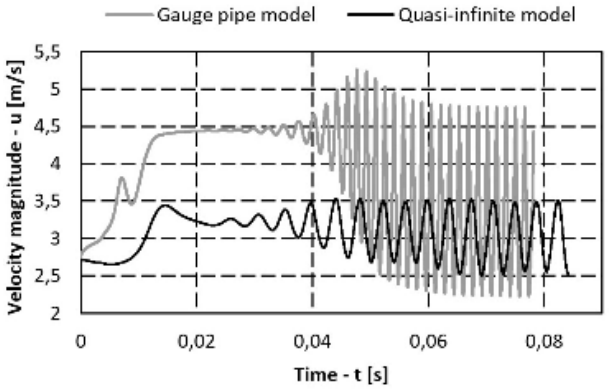

Fig. 8 Velocity magnitudes throughout the calculations

Vortex shedding frequencies (f_{sim}) for the simulations (*sim*) can be determined using the data measured in the monitor points. The Strouhal number (Str_{sim}) was calculated according to Eq. (2). The results of the preliminary investigation are shown in Table 3.

In accordance with the related literature [10, 11], the results of the preliminary investigation have shown, that there is a significant difference in the vortex shedding frequencies for the given cases, thus further numerical simulations with different velocity magnitudes were carried out using the model of the gauge pipe. Time steps for these simulations were determined individually in order to keep the Courant number below 1.

Table 3 Results of the preliminary investigation

Name	Infinite	Gauge pipe	Unit
f_{sim}	268.82	619.6	[Hz]
Str_{sim}	0.138	0.317	[-]

3.5 Validation of present results

As the present numerical analysis was performed using the commercial software ANSYS Fluent, it is required to establish the validity of the results. As mentioned in 3.2, measurement results are available for the infinite model in [2], which can be used for validation. Fig. 9 shows the relationship between the Strouhal and Reynolds numbers for the additional simulations carried out on the model of the gauge pipe, measurement results from a broad flow-field setup [2], and the result of the preliminary simulation using the infinite model.

When comparing the measurement and simulation results for the infinite model, the relative error is 0.73 %, hence the results produced by the created simulation environment can be considered valid.

It has to be noted, that the numerical models were created using lengths measured from the original model of the flowmeter, using a device with an accuracy of ±0.02 mm. As having an influence on the accuracy of further calculations, these effects were also taken into account when calculating the uncertainties.

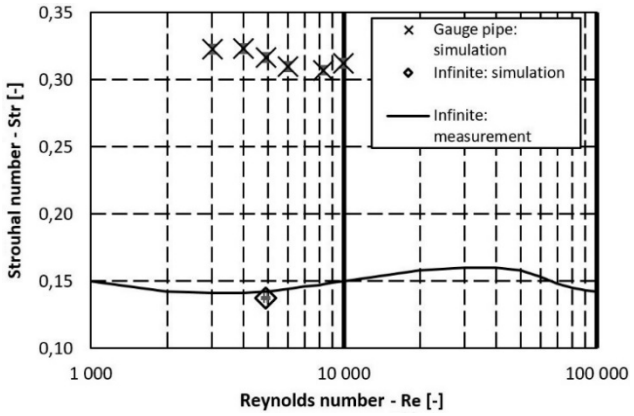

Fig. 9 Validation of the simulation results

3.6 Strouhal number

As stated before, simulations are used as a part of an alternative method to determine the vortex shedding frequency pertaining to the measurement results. If the device would be capable of displaying the vortex shedding frequency, this method would not be necessary, however, due to its limitations in its size, this function is not available.

For the method, a Strouhal and a Reynolds number is needed, by which the state of the flowmeter can be characterized in one of the calibration points. This pair of values – chosen (*ch*) from the results of the numerical simulations – are 4910 (Re_{ch}), and 0.317 (Str_{ch}). The velocity of the flow (u_{ch}) can be calculated using Eq. (1). The vortex shedding frequency (f_{ch}) can also be determined according to Eq. (2).

The volume flow rate (Q_{ch}) is calculated according to Eq. (7). From the data acquired via measurement, it can be determined, that between which two calibration values Q_{ch} falls. Knowing that every calibration value is matched with a value displayed by the flowmeter, it can also be determined what value of volume flow rate ($Q_{disp,\ ch}$) would the flowmeter be displaying, if it could be acquired during the measurement process. The described linear interpolation is shown in Fig. 10. $Q_{disp,\ ch}$ is calculated according to the formula presented in Eq. (8).

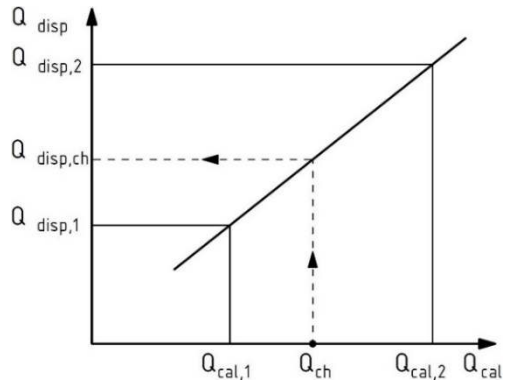

Fig. 10 Linear interpolation

$$Q_{disp,\ ch} = \frac{Q_{disp,\,2} - Q_{disp,\,1}}{Q_{cal,\,2} - Q_{cal,1}} \cdot \left(Q_{ch} - Q_{cal,1}\right) + Q_{disp,\,1} \tag{8}$$

Using this volume flow rate and f_{ch}, a proportionality factor (C) can be determined, shown in Eq. (9).

$$C = \frac{Q_{disp,\,ch}}{f_{ch}} \tag{9}$$

By multiplying any volume flow rate value measured by the instrument with C, it can be calculated what vortex shedding frequency (f_{disp}) the flowmeter would have displayed (Eq. (10)), thus the Strouhal number (Str_{disp}) can be determined (Eq. (2)). Final results are presented in Table 4.

$$f_{disp} = C \cdot Q_{disp} \tag{10}$$

Knowing the Reynolds and Strouhal numbers pertaining to the measurement results, their relationship can be examined. The Reynolds – Strouhal diagram for the data set obtained via the alternative method for the measurement results is shown in Fig. 11, together with the additional simulation results of the gauge pipe model formerly presented in Fig. 9.

Table 4 Final results

No.	Re	Q_{disp}	f_{disp}	Str_{disp}	Rel. error [%]	
	[-]	[l/min]	[Hz]	[-]	Re	Str_{disp}
1.	1 776	0.53	233	0.329	1.47	0.95
2.	3 026	0.89	389	0.322	1.39	0.92
3.	4 006	1.16	510	0.319	1.37	0.92
4.	4 910	1.41	620	0.317	1.37	0.91
5.	6 021	1.69	743	0.309	1.37	0.91
6.	7 264	2.01	883	0.305	1.37	0.92
7.	8 282	2.29	1 006	0.305	1.37	0.92
8.	9 192	2.61	1 147	0.307	1.37	0.91
9.	9 940	2.85	1 252	0.309	1.36	0.91
10.	10 619	3.06	1 345	0.311	1.36	0.91

The simulation and measurement results show good correlation, the coefficient of correlation is 0.974. The difference between each pair of points is within the band of uncertainty. Uncertainties of the Reynolds numbers are below 1.5 %, while for the Strouhal numbers, all values are below 1 %.

According to the measurement principle of the flowmeter, the trendline added to data sets presented in Fig. 11 should be horizontal, in order to achieve a constant behavior. However, when examining the tendencies on the diagram, a variation of the Strouhal number can be noticed throughout the measurement range of the instrument.

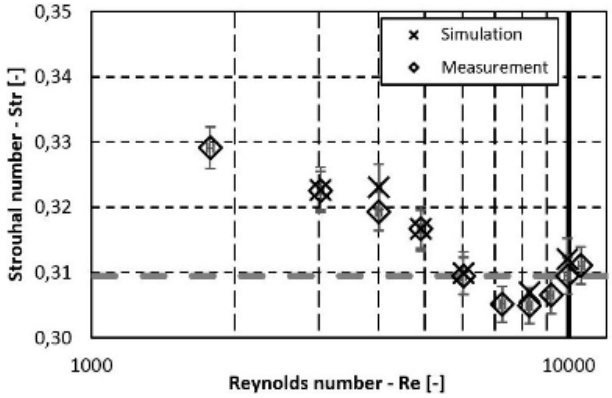

Fig. 11 Relationship of Reynolds and Strouhal numbers

The relative difference between the values measured using the calibration setup and the flowmeter was presented in Fig. 4. The accuracy of the flowmeter will be equal to the accuracy of the calibration rig, when the value of the relative difference is 0. According to Fig. 4, point No. 5 is the most accurate measurement point, hence the accuracy of the Strouhal number is also the highest in this point. In Fig. 11, a horizontal dotted line marks this value (0.309). Knowing this most accurate Strouhal number, the relative difference can be calculated for the remaining values with the formula in Eq. (11). Fig 13 reports the data from Fig. 4 together with the relative difference of the Strouhal number.

$$\varepsilon = \frac{0.309 - Str}{Str} \tag{11}$$

The correlation coefficient of the two data sets is 0.99, therefore it can be stated, that the variation of the Strouhal number has a major effect on the accuracy of the flowmeter.

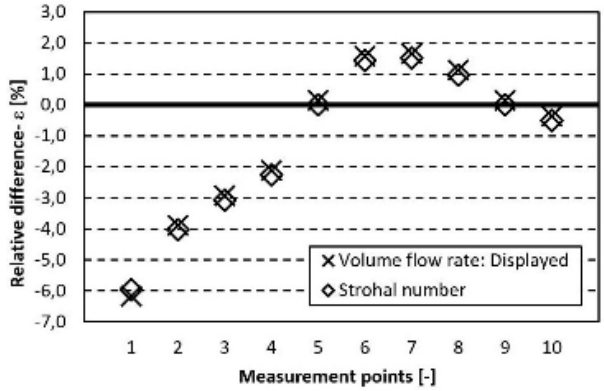

Fig. 12 Relative differences

4 Conclusion

In this study the nonconstant behavior of a vortex flowmeter with narrow gauge pipe was investigated. A calibration rig was designed and assembled, on which measurements were carried out. Preliminary results showed a noticeable nonconstant trend in the behavior of the device, which has been further investigated. While knowing the value of the vortex shedding frequency is essential in investigating whether the main measurement principle (Reynolds-Strouhal relationship) of the device is met, – due to the limitations caused by the narrow gauge pipe – it could not be measured directly. In order to determine the vortex shedding frequency, a diagnostic method was developed, combining numerical simulations and proportional calculations. In accordance with the literature regarding vortex meters with generally broad gauge pipes, the Reynolds – Strouhal diagram of this flowmeter has also shown, that the Strouhal number is not constant for the given Reynolds number range. By examining the relative difference of the measured values and relative difference of the Strouhal numbers, it was demonstrated, that the variation of the Strouhal number has a direct effect on the accuracy of the flowmeter. Further investigations can focus on the use of active and passive methods in order to increase the accuracy of vortex flowmeters with narrow gauge pipes. The active method is to reduce the variation of the Strouhal number by altering geometric properties of the gauge pipe and the bluff body. This can be achieved by carrying out further measurements and numerical simulations. If the Reynolds – Strouhal diagram of a certain flowmeter can be determined, the effects of the nonconstant behavior can be compensated during the data processing phase. By increasing the accuracy of the devices, further applications of vortex flowmeters can be achieved for various industrial purposes.

Acknowledgement

This work has been supported by the Hungarian National Research, Development and Innovation Centre under contracts No. K 112277.

The work relates to the scientific programs “Development of quality-oriented and harmonized R+D+I strategy and the functional model at BME” (Project ID: TÁMOP-4.2.1/B-09/1/KMR-2010-0002) and “Talent care and cultivation in the scientific workshops of BME” (Project ID: TÁMOP-4.2.2/B-10/1-2010-0009).

References

[1] Yoder, J. "Versatile flowmeter to see growth due to industry approvals." *Flow Control*. 16(12), pp. 48–49. 2010. [Online]. Available from: www.flowcontrol-digital.com [Accessed: 21st February 2017]

[2] Endress, U., Hafner, P., Jäggi, A., Kempf, G., Lang, M., Meyer, P., Schinke, A., Schulz, K., Sickinger, J., Silbermann, R., Steiner, K., Thommen, H., Tschabold, P., Wetzer, P., Zeller, E. "Vortex-Durchflussmessgeräte." In: *Durchfluss Fibel. 3. Ausgabe*, pp. 53-71. 1990. (in German)

[3] Hongjian, Z., Yongmei, H., Zhiqiang, S. "A study of mass flow rate measurement based on the vortex shedding principle." *Flow Measurement and Instrumentation*. 17, pp. 29-38. 2006. https://doi.org/10.1016/j.flowmeasinst.2005.08.002

[4] Okajima, A. "Strouhal numbers of rectangular cylinders." *Journal of Fluid Mechanics*. 123, pp. 379–398. 1982. https://doi.org/10.1017/S0022112082003115

[5] SMC Co. "3-color display digital flow switch for water-series PF3W." 2012. [Online]. Available from: www.smcworld.com [Accessed: 21st February 2017]

[6] ISO/IEC. "General requirements for the competence of testing and calibration laboratories." *ISO/IEC 17025:2005(E). Second edition*, pp. 1-28. 2005. Available from: www.iso.org [Accessed: 21st February 2017]

[7] Tanaka, M., Girard, G., Davis, R., Peuto, A., Bignell, N. "Recommended table for the density of water between 0 °C and 40 °C based on recent experimental reports." *Metrologia*. 38(4), pp. 301-309. 2001. https://doi.org/10.1088/0026-1394/38/4/3

[8] Moffat, R. J. "Using Uncertainty Analysis in the Planning of an Experiment." *Journal of Fluids Engineering*. 107(2), pp. 173-178. 1985. https://doi.org/10.1115/1.3242452

[9] Likhachev, E. R. "Dependence of water viscosity on temperature and pressure." *Technical Physics*. 48(4), pp. 514-515. 2003. https://doi.org/10.1134/1.1568496

[10] West, G., Apelt, C. "The effects of tunnel blockage and aspect ratio on the mean flow past a circular cylinder with Reynolds numbers between 10^4 and 10^5." *Journal of Fluid Mechanics*. 114, pp. 361-377. 1982. https://doi.org/10.1017/S0022112082000202

[11] Patil, P. P., Tiwari, S. "Effect of blockage ratio on wake transition for flow past square cylinder." *Fluid Dynamics Research*. 114(11-12), pp. 753-778. 2008. https://doi.org/10.1016/j.fluiddyn.2008.04.001

[12] Rahman, M. M., Karim, M. M., Alim, M. A. "Numerical investigation of unsteady flow past a circular cylinder using 2-D finite volume method." *Journal of Naval Architecture and Marine Engineering*. 4, pp. 27-42. 2007. https://doi.org/10.3329/jname.v4i1.914